Effects of Secondary Air on the Exhaust Oxidation of Particulate Matters

Pritchard, J., Cheng, W.K., SAE International Journal of Engines, 8 3 (2015)
SAE Paper 2015-01-0886

15PFL-0030

Effects of Secondary Air on the Exhaust Oxidation of Particulate Matters

Author, co-author (Do NOT enter this information. It will be pulled from participant tab in MyTechZone)
Affiliation (Do NOT enter this information. It will be pulled from participant tab in MyTechZone)

Abstract

The effects of secondary air on the exhaust oxidation of particulate matters (PM) have been assessed in a direct-injection-spark-ignition engine under fuel rich fast idle condition (1200 rpm; 2 bar NIMEP). Substantial oxidation of the unburned feed gas species (CO and HC) and significant reduction of both the particulate number (up to ~80%) and volume (up to ~90%) have been observed. The PM oxidation is attributed to the reactions between the PM and the radicals generated in the oxidation of the feed gas unburned species. This hypothesis is supported by the observation that the reduction in PM volume is proportional to the amount of heat release in the secondary oxidation.

Introduction

Direct injection (DI) is an attractive option for spark ignition (SI) engines. The fuel charge cooling improves the volumetric efficiency and knock margin so that highly boosted, downsized engines which offer substantial gains in fuel economy could be devised [1-4].

An important issue for DISI engines is the particulate matter (PM) emissions [5-9]. Particulate number (PN) emissions for small particles are especially of concern, as stringent limits have been established [10]. PN emissions during cold start in DISI engines are substantially higher than those in port-fuel-injection (PFI) engines [5, 6] because the in-cylinder fuel jet directly deposits liquid fuel on the cold cylinder walls. The fuel vapor that emerges from the fuel films produces fuel rich regions which are responsible for PM formation [5].

An effective strategy for controlling the tailpipe emission is to introduce secondary air injection to the exhaust [11-13]. Then, by running the engine rich and by retarding the spark timing substantially [14, 15], the secondary air would react with the exhaust mixture, thereby oxidizing the unburned hydrocarbons and enhancing the enthalpy flow to the catalyst. Thus both the tailpipe-out emissions before the catalyst light-off and the catalyst light-off time are reduced.

The interaction between the secondary air and the engine-out particulate matter is the subject of this paper. The issues being addressed are:

1. Would the secondary air injection strategy help to reduce the PM emission?
2. If so, to what extent is the PM emission reduced.
3. What is the mechanism behind this reduction?

Apparatus and procedure

Engine

The experiments were carried out in a production DISI engine (the GM LNF engine). The engine specifications are detailed in Table 1. The engine has cam phasers for both the intake and exhaust valves; the valve timings were fixed at the values given in Table 1. There was essentially no valve-overlap.

Table 1. Engine specifications for the GM 2L LNF DISI engine.

Engine type	Inline 4 cylinder
Displacement [cc]	1998
Bore [mm]	86
Stroke [mm]	86
Compression ratio	9.2:1
Fuel system	Side-mounted direct injection
Valve configuration	16 valve DOHC,
Intake valve open/close (0.25 mm lift)	1^o / 231^o (atdc-intake)
Exhaust valve /open close (0.25 mm lift)	-222 / 0^o (atdc-intake)
Max lift (both intake and exhaust)	10.3 mm

Operating condition

The engine operated at a condition typical of the cold fast idle period, at 1200 rpm and 2 bar net indicated mean effective pressure (NIMEP). The engine coolant temperature was regulated by a water chiller so that at the coolant inlet, the water temperature was at 20^o C.

The fuel used in these experiments was Haltermann HF0437 calibration gasoline with RON = 96.6 and RVP = 0.61 bar (9 psi). The fuel was supplied by a pressurized cylinder at 5 MPa. The fuel temperature was regulated by a single pass counter-flow shell-in-tube heat exchanger and was maintained at a temperature of 20°C.

The start of the direct fuel injection was at 80^o aTDC-intake. This timing was chosen so that there was a significant amount of PM in the exhaust while the amount did not change rapidly with respect to the injection timing.

Secondary air injection

The secondary air injection (SAI) arrangement is shown in Fig. 1. The secondary air flow rate was controlled by the air injection pressure through critical orifices. An end-plugged 3.2 mm (1/8") OD tube with two 1.6 mm holes drilled cross-wise supplied the secondary air to each branch of the exhaust port. The air flow was perpendicular to the exhaust flow to promote mixing [16]. The air injection points were at 2 cm from the exhaust valve seat. Pictures of the injection arrangement are shown in Fig. 2.

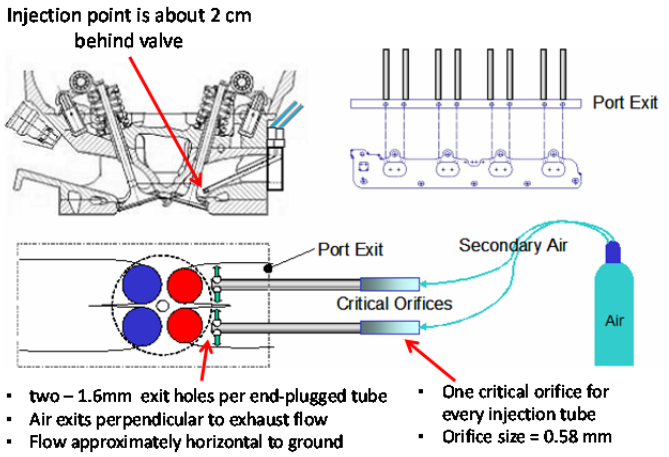

Figure 1. Secondary air injection arrangement

Figure 2. Secondary air injection hardware

Table 2. Representative secondary air flow value.

Representative running condition	
$\lambda_{engine}/\lambda_{exhaust}$	0.8 / 1.0
Spark	15° atdc-compression
Speed/ NIMEP	1200 rpm / 2 bar
Representative secondary air flow	
Total (8 tubes)	198 SLPM; corresponds to 4.2 g/s
Per tube	24.8 SLPM; corresponds to 0.53 g/s
Velocity at exit hole	100 m/s
Volume occupied by injected air during EVC	0.03 L
Length of runner occupied by the above air	4 cm

The amount of secondary air was metered by the λ value measured at the exhaust (i.e. the λ value after the engine-out exhaust gas mixed with the secondary air). The representative secondary air flow is shown in Table 2. The air exit velocity was fast (~100 m/s) to enable fast mixing. Note that the secondary air injection was continuous, while the engine exhaust flow for each cylinder is intermittent. The length of the exhaust runner occupied by the injected air during exhaust valve close was approximately 4 cm. This slug of air would mix with the burned gas of the next cycle and with that from the other cylinders. Therefore the actual mixing process is substantially non-uniform in nature.

Particle Measurements

The particle size spectrum was measured by a scanning mobility analyzer (TSI SMPS Model 3934). Each measurement took a scan time of 90 seconds with the engine running at steady state condition. The sampling location was at approximately 1 m downstream of the turbine to allow adequate time for the secondary air to mix and react with the exhaust stream. The catalyst has been taken out in these experiments. The sampling was done via a heated sample line and the sample was diluted by nitrogen. The dilution ratio was determined by measuring the CO_2 concentration at the sampling inlet with a Horiba MEXA 584L CO_2 meter, and at the SMPS inlet by a more sensitive Licor LI-820 CO_2 analyzer. The sampling system was heated to 200° C to prevent condensation. Because there were significant pressure pulsations at the sampling inlet, to maintain a steady sampling flow to the dilution system, a heated "T" design similar to that used in the fast-response HC analyzers [17] was used. The details have been described in Ref. [5].

Because of the presence of secondary air, the particulate matter concentrations have been corrected for both the dilution ratio and the temperature and pressure, and are reported as the undiluted values at the sampling inlet adjusted to the reference temperature of 300K and pressure of 1 bar.

Temperature Measurements

To determine the heat release from the secondary air reaction with the exhaust gas, the temperatures of the exhaust stream were measured at the locations shown in Fig. 3. The measurements were done with type K thermocouples inside a shielded aspiration probe to minimize radiation loss [18]. To estimate the heat loss in the different sections of the exhaust system, the wall temperatures were measured by an IR radiation thermometer.

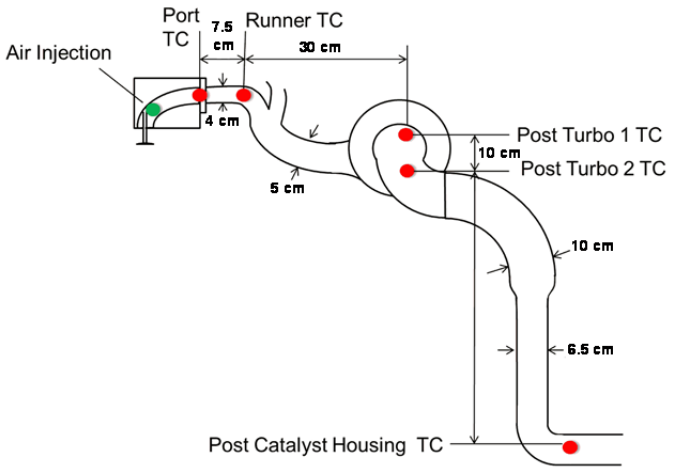

Figure 3. Locations of temperature measurements for assessing the heat release from the reaction of secondary air and the engine exhaust gas

Heat Release from the Secondary Air and Exhaust Gas Reaction

The strategy was to run the engine rich (at engine λ= 0.8 and 0.9) to provide an engine-out feed-gas with significant chemical enthalpy, and then to oxidize this gas by the secondary air to enhance the sensible enthalpy flow. The in-cylinder air equivalence ratio will be referred to as the engine λ; the air equivalence ratio of the mixture of feed gas and secondary air will be referred to as the exhaust λ. Thus the difference between the exhaust λ from the engine λ is a measure of the amount of secondary air injection.

The feed-gas chemical enthalpy was obtained by measuring the CO and HC concentrations at the entry of the exhaust runner of cylinder #4; the H2 concentration was not measured but was calculated from the water gas shift equilibrium at 1740K. The values are shown in Table 3. The chemical enthalpy at λ = 0.9 was ~500 kJ/kg-exhaust gas, and at λ = 0.8 was ~ 1000 kJ/kg-exhaust gas. In comparison, the exhaust sensible enthalpy was approximately 1000 kJ/kg-exhaust gas.

Table 3. Engine out chemical enthalpy at 1200 rpm, 2 bar NIMEP. Exhaust sensible enthalpy ~1000 KJ/kg-exhaust gas.

Engine λ	Spark Timing [aTDC]	Feed-gas chemical enthalpy [kJ/kg exhaust]	Percent Enthalpy Contribution		
			CO	H2	HC
0.9	10	520	63%	16%	21%
0.9	15	510	64%	17%	19%
0.8	10	1070	65%	20%	15%
0.8	15	1050	66%	21%	14%

The CO and HC concentrations in a mixing tank approximately 1.5 m downstream from the turbine were measured. It was assumed that beyond this location the temperature was sufficiently low such that there was no further reaction between the secondary air and the exhaust. These values, referred to as the exhaust values, were corrected for the secondary air dilution, and therefore, were measures of the extent that the feed gas species were oxidized. These exhaust CO and HC mole fractions are shown in Figures 4 and 5. At exhaust λ equal to engine λ, there was no secondary air. Since the engine was operating rich, there was little oxygen in the exhaust stream; hence there was little oxidation of the CO and HC. As more secondary air was introduced (increase in exhaust λ), there was increasing oxidation. Beyond exhaust λ of 1.05, most of the CO and HC were oxidized.

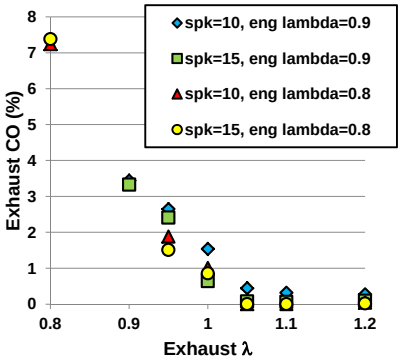

Figure 4. Exhaust CO mole fraction (corrected for secondary air dilution) as a function of the exhaust λ for various engine λ and spark timing. Engine operated at 1200 rpm and 2 bar NIMEP.

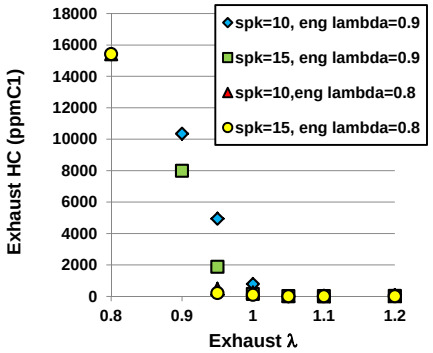

Figure 5. Exhaust HC mole fraction (corrected for secondary air dilution) as a function of the exhaust λ for various engine λ and spark timing. Engine operated at 1200 rpm and 2 bar NIMEP.

The temperature measurements at the locations shown in Fig. 3 are shown in Figures 6 and 7 for engine λ = 0.9 at spark timing of 10° and 15° aTDC. When no SAI was used (exhaust λ = engine λ), the temperature decreases downstream due to heat loss. When SAI was applied, the decrease was less because of the heat release from the secondary reactions. The effect was more prominent at spark timing of 15° aTDC for which the exhaust temperature was higher so that the heat release reaction was faster.

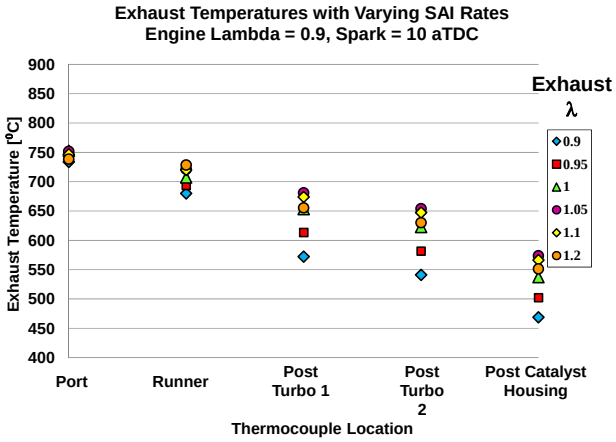

Figure 6. Exhaust gas temperatures at locations (shown in Fig. 3) for engine λ =0.9 and varies exhaust λ values; spark timing at 10° aTDC.

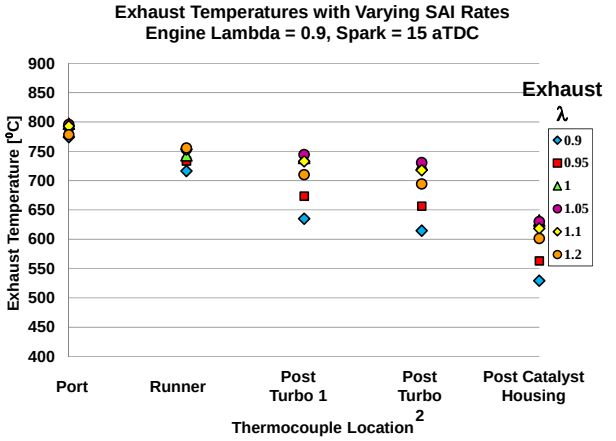

Figure 7. Exhaust gas temperatures at locations (shown in Fig. 3) for engine λ =0.9 and varies exhaust λ values; spark timing at 15° aTDC.

The effect of the secondary heat release on the exhaust gas temperature was most prominent when the engine λ was substantially rich; see Figures 8 and 9 for engine λ =0.8. Because of the significant secondary heat release, the exhaust temperature increased downstream first and then decreased when the effect of heat loss took over.

It is observed that for all the test cases, the exhaust temperature was highest when the exhaust λ ~1 to 1.05. At lower exhaust λ, there was insufficient air to complete the secondary oxidation. At higher exhaust λ, the excess secondary air diluted the exhaust gas and lowered the temperature. That the highest temperature occurred at exhaust λ slightly higher than 1 was because of the incompleteness of mixing so that more air than was stoichiometricly required was needed to complete the oxidation of the feed gas unburned species.

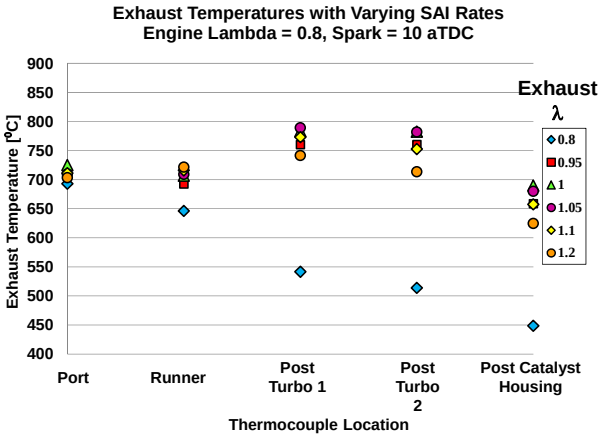

Figure 8. Exhaust gas temperatures at locations (shown in Fig. 3) for engine λ =0.8 and varies exhaust λ values; spark timing at 10° aTDC.

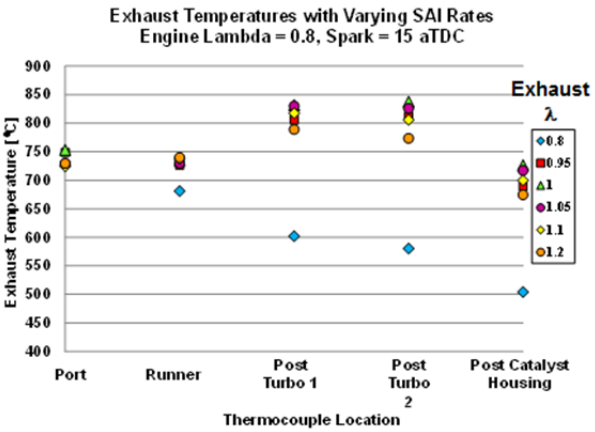

Figure 9. Exhaust gas temperatures at locations (shown in Fig. 3) for engine λ =0.8 and varies exhaust λ values; spark timing at 15° aTDC.

The amount of heat release from the secondary air reaction with the exhaust gas for the various zones bounded by the temperature measurements may be obtained from heat balance. The heat release rate $\dot{Q}_i$ of zone i may be obtained by energy balance:

$$\dot{Q}_i = \dot{m}(h_{out} - h_{in}) + \frac{T_i - T_w}{R_i} \qquad (1)$$

Here, $\dot{m}$ is the mass flow rate; h_{in} and h_{out} are the sensible enthalpies calculated from the measured inlet and outlet temperatures of the zone; T_i is the gas temperature taken as the average of the inlet and outlet temperatures; T_w is the wall temperature obtained from the IR radiometer measurements; and R_i is thermal resistance for heat loss to the wall. The value of R_i is calibrated by using Eq. (1) with the measurements taken without secondary air, for which there is negligible $\dot{Q}_i$.

It is assumed that beyond the exhaust gas sampling point (in a mixing tank located at 1.5 m downstream of the turbine), there is no further secondary oxidation because of the substantial heat loss in the exhaust system. Therefore the exhaust chemical enthalpy is a measured of the incompleteness of the secondary oxidation. The CO and HC concentrations were measured. The H_2 value was not. The H_2 concentration for the no SAI case was calculated from the water gas shift equilibrium at 1740K. The values for the cases with SAI were estimated by assuming that the extent of the H_2 oxidation was the same as that of CO.

Fig. 10 shows the heat release in each zone as percentages of the feed gas chemical enthalpy for a typical SAI case (engine λ = 0.9; exhaust λ = 1.05; spark timing at 10° aTDC). The heat release for Zones 1-4 were calculated with the procedure described in the above. For Zone 0, where the inlet temperature was not known; the heat release was estimated as the balance between the overall chemical enthalpy released (the difference between the feed gas chemical enthalpy and the exhaust chemical enthalpy), and the total heat release in Zones 1-4. Note that there is a slight systematic error due to the plausibility of a small amount of secondary heat release from the exit of Zone 4 to the exhaust sampling point if the temperature beyond Zone 4 is sufficiently high.

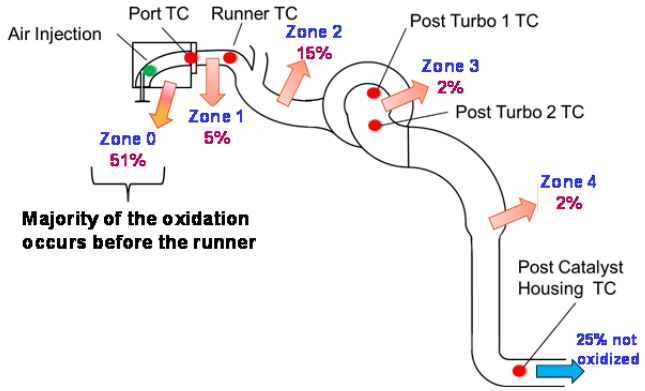

Figure 10. Typical zonal secondary heat release as percentage of the overall heat release from secondary oxidation. For this case, engine λ =0.9; exhaust λ =1.05; spark timing at 10° aTDC.

The zonal heat release as a fraction of the feed gas chemical enthalpy may be used as the measure of extent of secondary oxidation. The values for the cumulative zonal secondary oxidation are shown in Fig. 11 for engine λ = 0.9 and in Fig. 12 for engine λ = 0.8. The major part of the oxidation occurred in Zone 0, where the secondary air was introduced to the hot exhaust gas. The amount of oxidation beyond the turbocharger (Zone 2) was comparatively small. The total oxidation increases with spark retard and with decrease of engine λ. At engine λ = 0.8 and with exhaust λ > 1, oxidation of the exhaust species was almost complete.

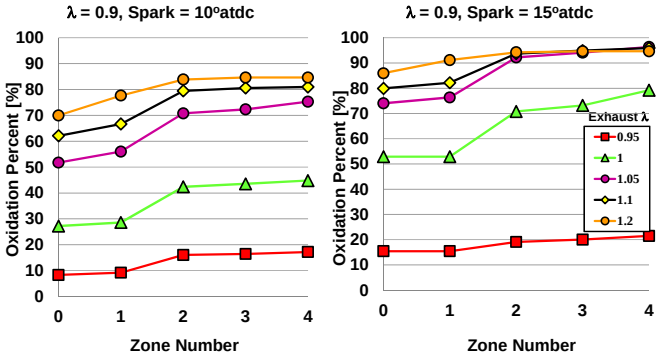

Figure 11. Cumulative zonal oxidation (heat release as % of feed gas chemical enthalpy) for engine λ =0.9 and various SAI levels as indicated by the exhaust λ.

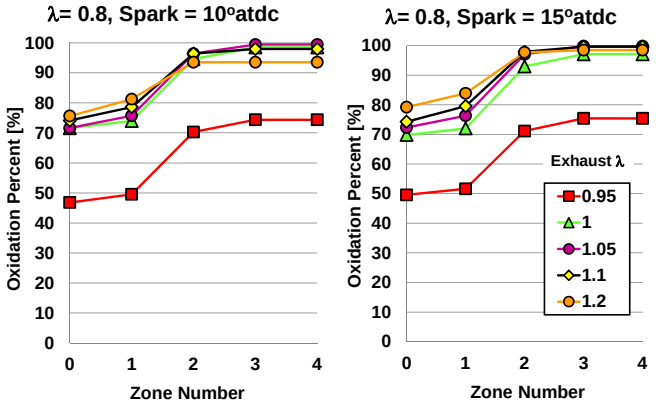

Figure 12. Cumulative zonal oxidation (heat release as % of feed gas chemical enthalpy) for engine λ =0.8 and various SAI levels as indicated by the exhaust λ.

Particulate oxidation

The particle size spectra for the four run conditions are shown in Figures 13-16. The particle numbers (PN) have been corrected for dilution and for temperature and pressure; they are reported in terms of number of particles per standard cm^3, with the standard condition being 300K and 1 bar.

Since the engine operated under rich condition, when SAI was not used, there was little oxidation in the exhaust system. The PN values measured in the exhaust (approximately 1 m down stream from the turbine) may be taken as the feed gas values. Therefore the difference between the PN for the various exhaust λ cases and that for the case with exhaust λ-equal-engine λ is a measure of the secondary PM oxidation.

There was significant secondary PM oxidation. The PN values decrease over the entire size spectrum with increase amount of secondary air. The decrease was most pronounced when the engine operated under the richer condition (engine λ =0.8). There was a diminishing return on the magnitude of reduction when the exhaust λ went beyond stoichiometric.

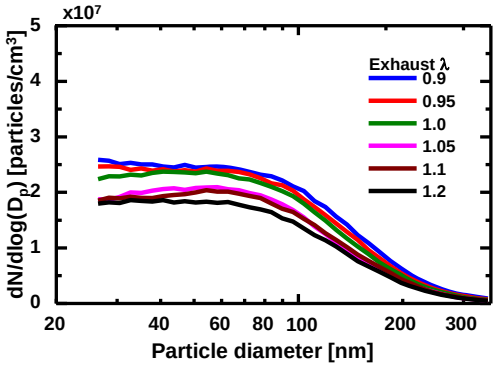

Figure 13. Particulate size distribution at engine λ =0.9 and spark timing of 10° aTDC for different levels of SAI as indicated by the exhaust λ values.

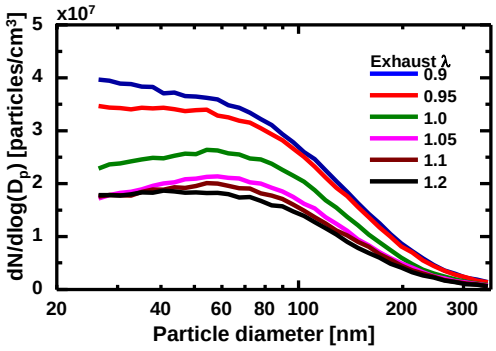

Figure 14. Particulate size distribution at engine λ =0.9 and spark timing of 15° aTDC for different levels of SAI as indicated by the exhaust λ values.

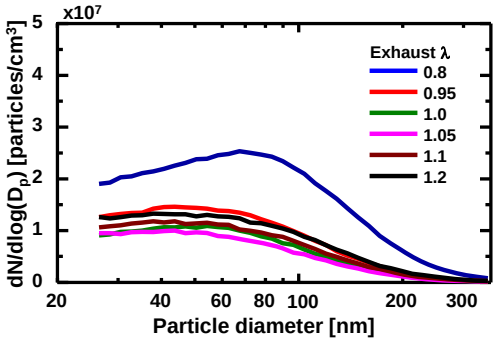

Figure 15. Particulate size distribution at engine λ =0.8 and spark timing of 10° aTDC for different levels of SAI as indicated by the exhaust λ values.

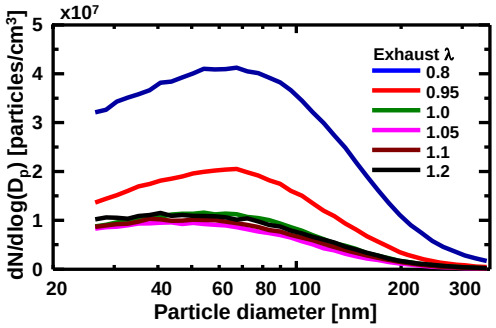

Figure 16. Particulate size distribution at engine λ =0.8 and spark timing of 15° aTDC for different levels of SAI as indicated by the exhaust λ values.

The total PN concentrations obtained by integrating the size spectrum over the range of 22 to 365 nm are shown in Fig. 17. The corresponding total particle volume concentrations (assuming that the particles are spherical) are shown in Fig. 18. Both the total PM number and volume decrease substantially with secondary oxidation; the maximum drop occurred at engine λ = 0.8, exhaust λ = 1.05, with the spark at 15° aTDC. No obvious correlation to the exhaust λ values is observed. The latter matter will be discussed later section.

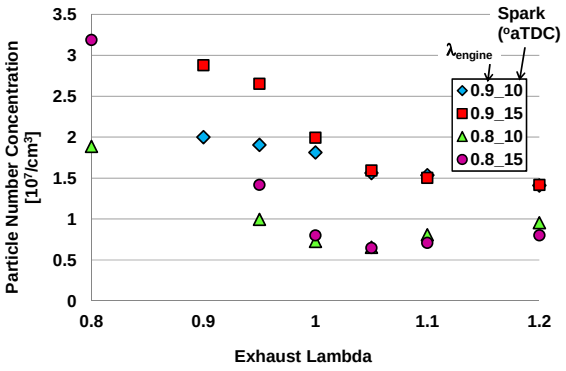

Figure 17. Total particulate number concentration (integrated over the size range of 22 to 365 nm) as a function of exhaust λ.

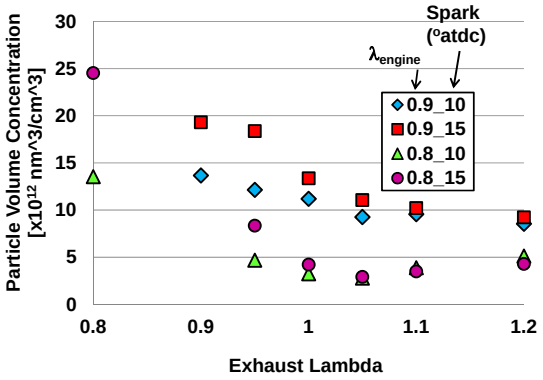

Figure 18. Total particulate volume concentration (integrated over the size range of 22 to 365 nm) as a function of exhaust λ.

Discussion

Oxidation mechanism

The Strickland-Constable formula for soot oxidation was used to assess the degree of PM oxidation in the exhaust with SAI. Assuming spherical particles, the surface oxidation rate can be converted to a particle radius recession rate [19]. This rate is plotted in Fig. 19 as a function of temperature and the amount of secondary air as indicated by the exhaust λ. For the Strickland-Constable calculation used in this plot, the temperature is an independent variable; the oxygen amount is calculated from the exhaust λ value. For a given exhaust λ, the recession rate increases almost exponentially with temperature and then decreases with temperature due to a change of the oxidation mechanism [19].

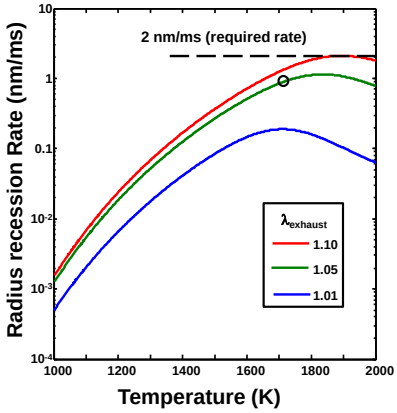

Figure 19. Particle radius recession rate due to secondary oxidation according to Strickland Constable formula, as a function of temperature and secondary air. The circle marks the maximum radius recession rate at engine λ = 0.8.

For the same temperature, the radius recession rate always increases with exhaust λ because more oxygen is available. In the engine experiment, however, the temperature and exhaust λ are not independent. A higher exhaust λ value beyond stoichiometric would lead to a lower temperature because of dilution. Therefore, the maximum particle radius recession rate is achieved via a tradeoff between temperature and available oxygen. In the appendix, the maximum rate based on adiabatic condition is estimated to be achieved at an exhaust λ of 1.05 according to the tradeoff between temperature and available oxygen. This value, marked on Fig. 19, is ~ 1 nm / ms.

The exhaust gas residence time at the test condition is estimated to be ~20 ms. Therefore, to oxidize an 80 nm diameter particle, the radius recession time should be greater than 2 nm / ms. This rate is higher than the estimated rate under the most favorable assumptions (adiabatic and instantaneous secondary heat release); see Fig. 19. Therefore, the Strickland-Constable oxidation model is deemed not sufficient for explaining the results.

It is noted that the Strickland-Constable model has been based on data from graphite oxidation in oxygen. In the oxidation process in the engine exhaust, the secondary air reacts with the CO, hydrogen and HC in the feed gas so that there are significant presence of intermediate radicals such as OH and O. These radicals, especially in the case of oxidation of the absorbed HC on the particles, would be in the proximity of the particles and oxidize the particles.

To examine the validity of the above explanation, the total particle volume reduction percentage is plotted against the exhaust enthalpy release for the secondary reaction in Fig. 20. The latter quantity has been calculated as the difference between the feed gas chemical enthalpy and the exhaust gas chemical enthalpy. That all the data points in Fig. 18 now collapse as a straight line passing through the origin gives strong support of the above explanation.

The corresponding particle number reduction is shown in Fig. 21. Note that the particle volume reduction was almost up to 90% and number reduction was up to 80% at the maximum secondary heat release point at engine λ = 0.8, exhaust λ = 1.05 and spark timing of 15° aTDC.

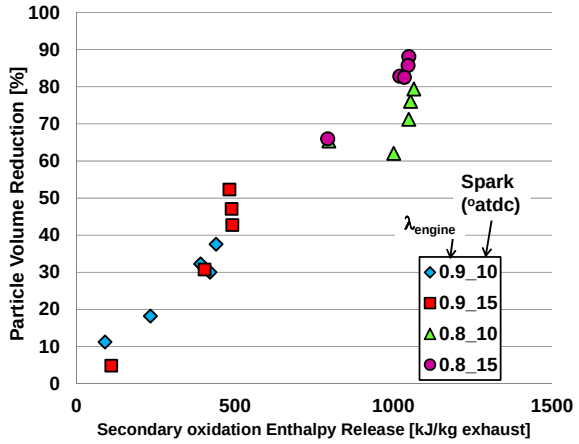

Figure 20. Particle volume reduction as a function of the enthalpy release by secondary oxidation; all data included.

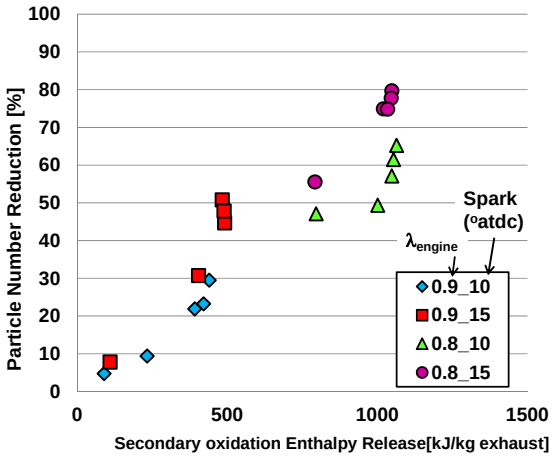

Figure 21. Particle number reduction as a function of the enthalpy released by secondary oxidation.

Summary/Conclusions

The effects of secondary air on the exhaust oxidation of particulate matters have been assessed in a SIDI engine under fast idle condition (1200 rpm; 2 bar NIMEP). Secondary air was injected cross-wise in the exhaust port at 2 cm from the valves. The engine operated under fuel rich condition with engine λ = 0.8 and 0.9. The amount of secondary air was indicated by the exhaust λ which ranged from no secondary air (engine λ = exhaust λ) to exhaust λ = 1.2. The following conclusions are drawn:

1. There was significant oxidation of the unburned CO and HC by the secondary air. (The hydrogen concentration was not measured.)
2. The exhaust temperature was the highest at exhaust λ ~ 1-1.05. At lower exhaust λ, there was insufficient air to complete the secondary oxidation. At higher exhaust λ, the excess air diluted the exhaust gas and lowered the exhaust temperature. That the maximum occurred at exhaust λ slightly lean of stoichiometric was attributed to the incompleteness of the mixing process.
3. The secondary air was effective in reducing both the particulate number and the particulate volume. For the size range of 25-365 nm, up to almost 90% reduction of the particulate volume and 80% of particle number have been observed at engine λ = 0.8 and exhaust λ = 1.05 with spark at 15° aTDC.
4. The classical Strickland-Constable model for soot oxidation is deemed not adequate to explain the extent of secondary oxidation of the particulates. It is hypothesized that the particulate oxidation is via the radicals generated by the oxidation of the unburned species (CO, hydrogen and HC) from the feed gas.
5. The hypothesis is supported by the observation that the particulate volume reduction (in percent) is proportional to the enthalpy release from the secondary oxidation.

References

1. Bandel, W., Fraidl, G., Kapus, P., Sikinger, H. et al., "The Turbocharged GDI Engine: Boosted Synergies for High Fuel Economy Plus Ultra-low Emission," SAE Technical Paper 2006-01-1266, 2006, doi:10.4271/2006-01-1266.
2. Woldring, D., Landenfeld, T., and Christie, M., "DI Boost: Application of a High Performance Gasoline Direct Injection Concept," SAE Technical Paper 2007-01-1410, 2007, doi:10.4271/2007-01-1410.
3. Davis, R., Mandrusiak, G., and Landenfeld, T., "Development of the Combustion System for General Motors' 3.6L DOHC 4V V6 Engine with Direct Injection," SAE Int. J. Engines 1(1):85-100, 2009, doi:10.4271/2008-01-0132.
4. McNeil, S., Adamovicz, P., and Lieder, F., "Bosch Motronic MED9.6.1 EMS Applied on a 3.6L DOHC 4V V6 Direct Injection Engine," SAE Technical Paper 2008-01-0133, 2008, doi:10.4271/2008-01-0133.
5. Ketterer, J. and Cheng, W., "On the Nature of Particulate Emissions from DISI Engines at Cold-Fast-Idle," SAE Int. J. Engines 7(2):986-994, 2014, doi:10.4271/2014-01-1368.
6. Whitaker, P., Kapus, P., Ogris, M., and Hollerer, P., "Measures to Reduce Particulate Emissions from Gasoline DI engines," SAE Int. J. Engines 4(1):1498-1512, 2011, doi:10.4271/2011-01-1219.
7. Sabathil, D., Koenigstein, A., Schaffner, P., Fritzsche, J. et al., "The Influence of DISI Engine Operating Parameters on Particle Number Emissions," SAE Technical Paper 2011-01-0143, 2011, doi:10.4271/2011-01-0143.
8. Piock, W., Hoffmann, G., Berndorfer, A., Salemi, P. et al., "Strategies Towards Meeting Future Particulate Matter Emission Requirements in Homogeneous Gasoline Direct Injection Engines," SAE Int. J. Engines 4(1):1455-1468, 2011, doi:10.4271/2011-01-1212.
9. Peckham, M., Finch, A., Campbell, B., Price, P. et al., "Study of Particle Number Emissions from a Turbocharged Gasoline Direct Injection (GDI) Engine Including Data from a Fast-Response Particle Size Spectrometer," SAE Technical Paper 2011-01-1224, 2011, doi:10.4271/2011-01-1224.
10. Commission Regulation (EU) No 459/2012.
11. Borland, M. and Zhao, F., "Application of Secondary Air Injection for Simultaneously Reducing Converter-In Emissions and Improving Catalyst Light-Off Performance," SAE Technical Paper 2002-01-2803, 2002, doi:10.4271/2002-01-2803.
12. Koehlen, C., Holder, E., and Vent, G., "Investigation of Post Oxidation and Its Dependency on Engine Combustion and

Exhaust Manifold Design," SAE Technical Paper 2002-01-0744, 2002, doi:10.4271/2002-01-0744.
13. Lee, D. and Heywood, J., "Effects of Secondary Air Injection During Cold Start of SI Engines," SAE Int. J. Engines 3(2):182-196, 2010, doi:10.4271/2010-01-2124.
14. Hallgren, B. and Heywood, J., "Effects of Substantial Spark Retard on SI Engine Combustion and Hydrocarbon Emissions," SAE Technical Paper 2003-01-3237, 2003, doi:10.4271/2003-01-3237.
15. Russ, S., Thiel, M., and Lavoie, G., "SI Engine Operation with Retarded Ignition: Part 2 -HC Emissions and Oxidation," SAE Technical Paper 1999-01-3507, 1999, doi:10.4271/1999-01-3507.
16. Herrin, R., "The Importance of Secondary Air Mixing in Exhaust Thermal Reactor Systems," SAE Technical Paper 750174, 1975, doi:10.4271/750174.
17. Cheng, W.K., Summers, T., Collings, N., "The Fast- Response Flame Ionization Detector," Prog. in Energy and Comb. Sc., 24, 89-124, 1998.
18. Pritchard, J.J., "The Effects of Secondary Air Injection on Particulate Matter Emissions," MS Thesis, Dept. of Mech. E., MIT, February, 2014.
19. Heywood, J.B., *Internal Combustion Engine Fundamentals*, McGraw Hill, 1988.

Contact Information

Joseph Pritchard joe.j.pritch@gmail.com
Wai Cheng wkcheng@mit.edu

Acknowledgments

This work was supported by the Consortium for Engine and Fuels Research. The members of the Consortium were Chrysler, Borg Warner, Ford and General Motors.

Definitions/Abbreviations

aTDC	After top-dead-center
DI	Direct injection
DISI	Direct injection spark ignition
h	Enthalpy
HC	Hydrocarbon
IR	Infra-red
NIMEP	Net indicated mean effective pressure
PFI	Port fuel injection
PM	Particulate matter
PN	Particulate number
Q	Secondary heat release
R_i	Thermal resistance for heat loss
RON	Research octane number
RVP	Reid vapor pressure
SAI	Secondary air injection
SI	Spark ignition
SMPS	Scanning mobility particle spectrometer
T	Temperature

Appendix

Exhaust Temperature and PM Secondary Oxidation Consideration

A cycle simulation was used to assess the feed gas temperature and unburned gas species to the exhaust system. The adiabatic exhaust temperature with SAI, i.e. the temperature of the exhaust stream assuming complete reaction of the secondary air and the unburned feed gas species without heat loss is then calculated. The feed gas temperature as a function of the spark timing and engine λ is shown in Fig. A1. The adiabatic exhaust gas temperature as a function of feed gas temperature and amount of SAI for engine λ = 0.9 and 0.8 are shown in Figures A2 and A3 respectively. It is observed that although running at engine λ = 0.9 gives a higher feed gas temperature, a higher exhaust temperature is obtained by running the engine richer; at engine λ = 0.8 because then there is more heat release in the exhaust. The highest adiabatic exhaust temperature is obtained at exhaust λ =1, since there would not be any dilution of the exhaust by excess secondary air. However, then there is not sufficient oxygen to oxidize the PM. The best theoretical operating point for maximizing oxidation rate (see Fig. 19 of text) is at exhaust λ ~1.05 as a tradeoff between the available oxygen and the temperature. This point is marked in Fig. A3

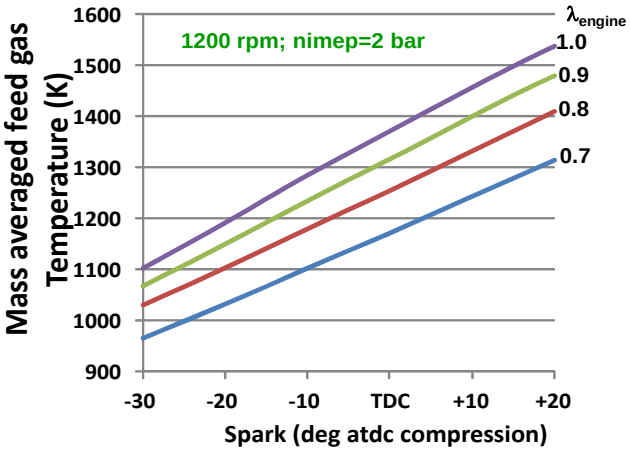

Fig. A1 Feed gas temperature (averaged over cycle) as a function of spark and engine λ.

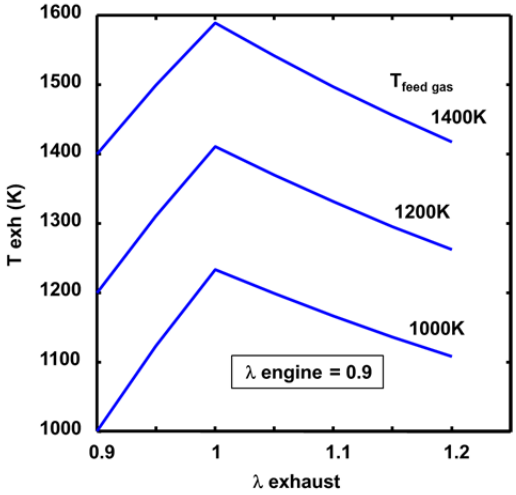

Fig. A2 Adiabatic exhaust gas temperature assuming complete oxidation of feed gas unburned species and secondary air, as function of feed gas temperature and amount of SAI (indicated by exhaust λ)

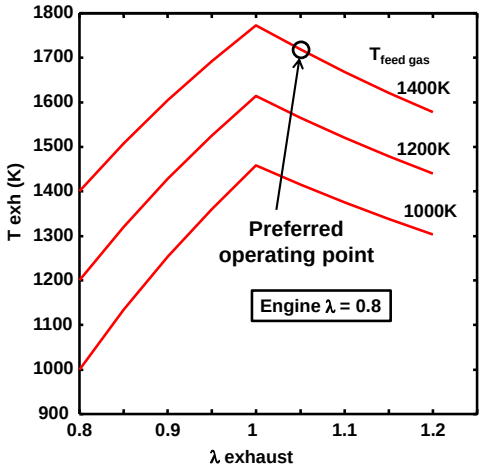

Fig. A3 Adiabatic exhaust gas temperature assuming complete oxidation of feed gas unburned species and secondary air; as function of feed gas temperature and amount of SAI (indicated by exhaust λ). Engine λ = 0.8.